Mechanisms and Cross Sections for Water Desorption from a Lunar Impact Melt Breccia

Alice DeSimone – Georgia Institute of Technology
Thomas M. Orlando – Georgia Institute of Technology

Citation of published version:
DeSimone, A., Orland, T. (2014): Mechanisms and Cross Sections for Water Desorption from a Lunar Impact Melt Breccia. *Journal of Geophysical Research*, 119(4).
DOI: https://doi.org/10.1002/2013JE004599

AGU PUBLICATIONS

JGR

Journal of Geophysical Research: Planets

RESEARCH ARTICLE
10.1002/2013JE004599

This article is a companion to *DeSimone and Orlando* [2014] doi:10.1002/2013JE004598.

Key Points:
- Photons of 157-nm desorb water deposited on a lunar impact melt breccia
- Cross sections for water removal were measured at 0.1–10 L H_2O exposures
- Photofragments of vibrationally excited water were detected

Correspondence to:
T. M. Orlando,
thomas.orlando@chemistry.gatech.edu

Citation:
DeSimone, A. J., and T. M. Orlando (2014), Mechanisms and cross sections for water desorption from a lunar impact melt breccia, *J. Geophys. Res. Planets*, *119*, 884–893, doi:10.1002/2013JE004599.

Received 19 DEC 2013
Accepted 14 MAR 2014
Accepted article online 18 MAR 2014
Published online 30 APR 2014

Mechanisms and cross sections for water desorption from a lunar impact melt breccia

Alice J. DeSimone[1] and Thomas M. Orlando[1,2]

[1]School of Chemistry and Biochemistry, Georgia Institute of Technology, Atlanta, Georgia, USA, [2]School of Physics, Georgia Institute of Technology, Atlanta, Georgia, USA

Abstract Desorption of H_2O ($v=0$) following 157-nm irradiation of amorphous solid water on a lunar impact melt breccia was measured with resonance-enhanced multiphoton ionization. Photofragments of vibrationally excited water were detected with nonresonant ionization. The average cross section for H_2O ($v=0$) removal and destruction at 0.1 Langmuir (1 L = 10^{-6} Torr·s) H_2O exposure was measured to be $(7.1 \pm 1.9) \times 10^{-19}$ cm^2. Cross sections were also measured at 0.3, 1, 5, and 10 L exposures. Because these cross sections increase drastically with decreasing water coverage, water is not expected to remain intact as H_2O on the sunlit lunar surface. Instead, photons are likely to cause H_2O to desorb or dissociate. The OH^+ fragment of H_2O (v^*) increased in intensity with increasing irradiation as hydroxyl groups built up on the surface and then recombined. The OH^+ signal eventually began to decrease after a dose of 5×10^{18} photons cm^{-2}. Under these conditions, the cross section for H_2O (v^*) photodesorption was measured to be 6.4×10^{-20} cm^2 for an initial exposure of 5 L H_2O.

1. Introduction

For several decades after the Apollo missions, the Moon was thought to be completely anhydrous. In recent years, however, H_2O and/or OH species have been discovered in permanently shadowed regions of the Moon [*Colaprete et al.*, 2010], in lunar volcanic glasses [*Saal et al.*, 2008], in lunar melt inclusions [*Hauri et al.*, 2011], and in anorthosites from the lunar magma ocean [*Hui et al.*, 2013]. Certain locations on the Moon seem to contain water with hydrogen isotope ratios similar to those found in comets, and it has been proposed that cometary water was delivered to the Moon shortly after it was formed [*Greenwood et al.*, 2011]. While it is possible that most of the Moon contained water in its distant past, the only evidence for water on the sunlit surface of the Moon today is infrared absorption near 3 μm [*Clark*, 2009; *Pieters et al.*, 2009; *Sunshine et al.*, 2009], which could be due merely to hydroxyl groups created by trapping of solar wind protons [*McCord et al.*, 2011; *Starukhina*, 2001, 2012]. Two of the primary causes of water depletion on the Moon's surface are photodesorption and photodissociation by solar photons.

Ultraviolet photons in the solar flux are able to excite H_2O to its first excited state, which is dissociative for an isolated water molecule. In the condensed phase, the first excited state becomes a band of $1b_1 \rightarrow 4a_1$ transitions with excitation energies of ~7–9.5 eV [*Kobayashi*, 1983]. Coupling to neighboring water molecules opens a pathway to intact desorption [*Chipman*, 2006]. However, significant dissociation still occurs when amorphous solid water (ASW) experiences irradiation, and a competition exists between dissociation and exciton delocalization, which facilitates desorption [*DeSimone et al.*, 2013; *Hahn et al.*, 2005]. Both desorption and dissociation from 157-nm irradiation of ASW have been studied experimentally and theoretically [*Andersson et al.*, 2011; *DeSimone et al.*, 2013; *DeSimone and Orlando*, 2014a; *Hama et al.*, 2009, 2010], but these previous studies probed thick ASW and did not involve the substrate.

In the present study, we investigate water desorption mechanisms and measure the water removal cross sections for 157-nm irradiation of thin ASW layers on a lunar impact melt breccia. In a recent paper [*DeSimone et al.*, 2013], we reported velocity distributions that support a dipole reversal mechanism for the desorption of H_2O from thick ASW. Direct excitation of a water molecule to its first excited state results in repulsive forces between the excited water molecule and its former hydrogen-bonding partners. Additionally, kickout by a hot hydrogen atom and recombination mechanisms were considered for the formation of vibrationally excited water molecules. Along with our complementary study of $O(^3P)$ formation by 157-nm irradiation of ASW on a lunar substrate [*DeSimone and Orlando*, 2014b], the present work aims to determine

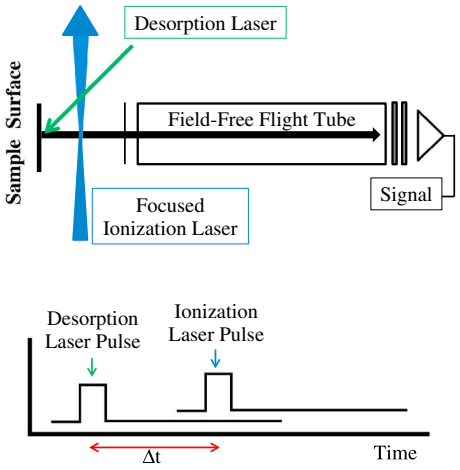

Figure 1. (top) Spatial and (bottom) temporal diagrams of the two-laser REMPI-TOF experimental setup. The unfocused 157-nm desorption laser beam strikes the sample at a 45° angle. After a brief delay time (Δt), the focused ionization laser beam passes through the desorption plume. Positive ions produced by the ionization laser are accelerated toward the field-free flight tube by a positive voltage on the sample and a negative voltage on the TOF extractor.

whether the same mechanisms are in effect for thin ASW layers on a lunar substrate. H_2O has been desorbed by 157-nm irradiation from ASW on a lunar substrate and detected by resonance-enhanced multiphoton ionization (REMPI). Rotational and translational energies of the desorbed water molecules have been determined by comparison with simulations, and cross sections for water removal have been measured for various H_2O exposures.

2. Experiments and Data Analysis

2.1. Laboratory Measurements

Photodesorption experiments were performed in an ultrahigh vacuum chamber with a base pressure of 2×10^{-10} Torr. The chamber was equipped with a leak valve for dosing water, a time-of-flight (TOF) mass spectrometer, and a liquid-nitrogen-cooled copper sample holder. The lunar substrate was an impact melt breccia collected during Apollo 16 (NASA sample 60017.196). The impact melt breccia was probably produced by a basin-forming impact that brought mafic material and KREEP (potassium, rare earth elements, and phosphorous) from beneath the crust to the surface and crushed this material into a heterogeneous aluminosilicate glass [*Korotev*, 2000]. One side of the slab was cut smoothly, and this flat side was pressed against the copper sample holder with tantalum strips to make cooling and heating possible. All experiments were performed at the minimum sample temperature, 102 K, unless otherwise stated.

Unfocused 157-nm light from an excimer laser (GAM Laser, EX5) entered the chamber through a nitrogen-purged path and a magnesium fluoride window and struck the sample at a 45° angle. Excimer laser energies were typically 150–350 μJ cm^{-2} per pulse. For low-coverage experiments, background dosing was performed at a water pressure of 1×10^{-8} Torr, resulting in 0.1 L (1 Langmuir = 1×10^{-6} Torr · s) for 10 s of exposure. For high-coverage experiments, background dosing was performed at 5×10^{-8} Torr H_2O, resulting in 30 L for 10 min of exposure. With unity sticking probability, 1 L exposure roughly corresponds to a film thickness of 1 monolayer (ML). However, the large hit-and-stick probability at 102 K leads to small cluster growth. As water adsorbs by cluster formation, the exact relationship between exposure and thickness is unknown, but 1 L exposure likely corresponds to between 0.3 and 1 ML of water [*Sato et al.*, 2000].

Desorbed water molecules were detected with 2 + 1 REMPI on the C(000) ← X(000) transition. This transition corresponds to wavelengths 247.8–248.6 nm, which were obtained by frequency doubling the visible output of a neodymium: yttrium/aluminum/garnet-pumped optical parametric oscillator (Spectra-Physics, MOPO-SL). The ionization beam was 2 ± 0.5 mm above the surface with a focal volume of ~10 μm^3. The distance between the surface and the detection region was not exactly constant due to the surface roughness.

The time between desorption and ionization laser pulses was varied with a delay generator from 0 to 8 μs to probe different parts of the desorption plume time-of-flight (TOF) distribution. This delay time equals the flight time of the molecule from the surface to the detection region. The water peak in each mass spectrum was integrated to obtain the total signal for each time delay, and the graph of total signal versus time delay became the total TOF spectrum. Diagrams illustrating the laser alignment and timing of this experiment are shown in Figure 1.

To determine water removal cross sections (σ), water signal was plotted versus number of incident 157-nm photons and the data were fit with exponential functions of the form $y = Ae^{-\sigma x}$, where x has units of

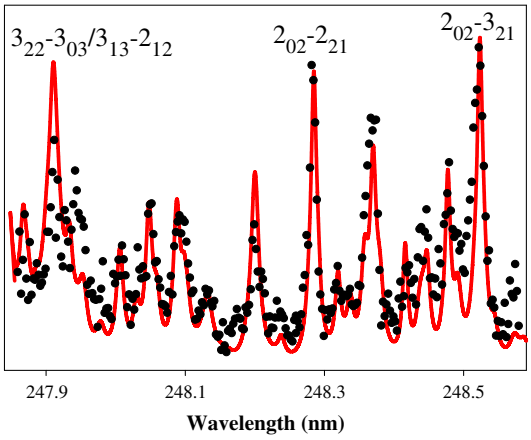

Figure 2. A 2 + 1 REMPI spectrum of water desorbed from from 1 L ASW at 102 K on the lunar slab by 157-nm irradiation. The red line is a simulated spectrum with a rotational temperature of 300 K.

photons cm^{-2}. The number of 157-nm photons was calculated using the pulse counter on the excimer laser display, average excimer power measured before and after the scan, and a correction factor of 0.65 for losses passing through the MgF_2 window.

Detecting vibrationally excited water molecules by REMPI at 251.8–253.8 nm, where the H_2O(C-X) $\Delta v_2 = -1$ transitions occur [*Andersson et al.*, 2011], was not possible, probably due to predissociation. However, TOF spectra for the fragment ions of vibrationally excited water molecules, H^+ and OH^+, were obtained at 253.0 nm with a distance of 3.5 ± 0.5 mm between the surface and the detection region. Because the vibrationally excited water molecules do not fragment until absorbing additional photons in the detection region, TOF measurements of the fragment ions actually probe the velocities of the parent molecules [*DeSimone et al.*, 2013]. OH^+ signal at the peak of its TOF spectrum was then monitored as a function of irradiation time, and a cross section for H_2O (v^*) removal was calculated, assuming that the entire OH^+ signal was in fact due to H_2O (v^*).

2.2. Simulation of TOF, Velocity, and REMPI Spectra

Simulation of the TOF spectrum involved flux-weighted Maxwell-Boltzmann distributions, which are appropriate for photodesorption of chemisorbed species [*Zimmermann and Ho*, 1995]. The H_2O ($v = 0$) TOF spectrum was fit adequately by the sum of three Maxwell-Boltzmann distributions, $S(t, T_{trans})$, of the following form:

$$S(t, T_{trans}) = At^{-4} \exp\left(\frac{-mr^2}{2k_B T_{trans} t^2}\right), \quad (1)$$

where T_{trans} is the translational temperature, r is the distance between the surface and the detection region, and A is a scaling factor.

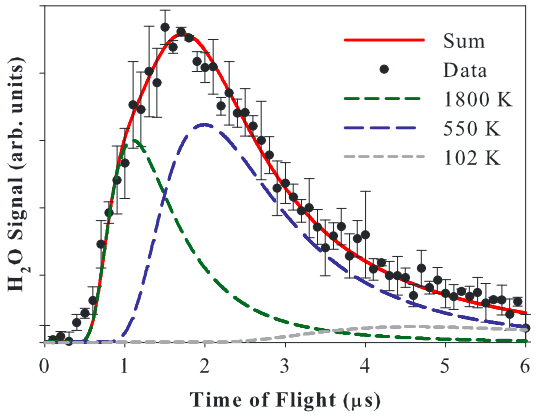

Figure 3. TOF spectrum for H_2O desorbing from 2 L ASW on lunar slab at 102 K due to 157 nm irradiation. Maxwell-Boltzmann distributions with $r = 2.0$ mm and $T_{trans} = 1800$, 550, and 102 K sum to fit the data.

TOF data were also plotted in velocity space using the Jacobian transform, $P_v(v) = tr^2 S(t)$, where $v = r/t$ and $S(t)$ is the measured signal intensity at each time. The velocity distribution was also fit with a sum of three Maxwell-Boltzmann distributions of the following form:

$$P_v(v, T_{trans}) = Av^3 \exp\left(\frac{-mv^2}{2k_B T_{trans}}\right), \quad (2)$$

where the values of T_{trans} were equal to those used to fit the TOF spectrum.

The 2 + 1 REMPI spectrum of H_2O was simulated with PGOPHER, a freely available program for simulating rotational spectra. (PGOPHER, a Program for Simulating Rotational Spectra, C. M. Western, University of Bristol, http://pgopher.chm.bris.ac.uk.) More

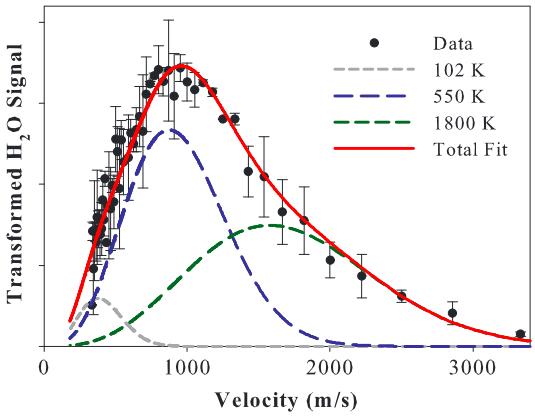

Figure 4. Velocity distribution for H_2O desorbing from 2 L ASW on lunar slab at 102 K due to 157-nm irradiation. Maxwell-Boltzmann distributions with $r = 2.0$ mm and $T_{trans} = 1800$, 550, and 102 K sum to fit the data.

details about this procedure are available in our previous work [*DeSimone et al.*, 2013].

3. Results

The 2 + 1 REMPI spectrum of desorbed water from 1 L ASW at 102 K on the lunar slab exhibited rotational excitation, with a rotational temperature of 300 ± 75 K. For thick ASW, the rotational temperature was 425 ± 75 K [*DeSimone et al.*, 2013], but the data were quite similar. The true value may be 350–375 K, and unavoidable fluctuations in laser powers may be responsible for the slight differences in peak heights. The spectrum shown in Figure 2 was created by scanning a 0.2 nm interval in 0.0025 nm increments, averaging data from 64 laser pulses at each wavelength. A fresh 1 L of water was dosed prior to each 0.2 nm interval to avoid signal decreasing as coverage decreased. Each data point shown is the average of the signal from at least two scans with different starting wavelengths. In determining the temperature of best fit, least emphasis was placed below 248 nm because the ionization laser power was not stable at those wavelengths.

The shape of the H_2O TOF spectrum from ASW on the lunar slab was found to be independent of H_2O exposure (from 1 to 20 L), desorption laser flux, and ionization energy. Figure 3 shows the TOF spectrum for H_2O desorbing from 2 L ASW on the lunar slab and the three Maxwell-Boltzmann components calculated according to equation (1) with $r = 2$ mm that sum to the total fit. The TOF spectrum was very similar to that of desorbed water from thick ASW dosed directly onto the sample holder, except that the spectrum from the lunar slab was wider. Due to water desorbing from within pores in the lunar slab, a small thermal component at 102 K was added to account for some of the extra width. The flight distance (r) was 2.0 ± 0.5 mm based on careful laser alignment. If a larger thermal component were present, a more precise value of r could be determined by fitting the thermal component best at 102 K, but the thermal component was too small compared to the other components for this purpose. Since both r and T_{trans} primarily shift the spectrum horizontally on the time axis, the resulting uncertainties in translational temperatures are $T_{trans,1} = 1800 \pm 700$ K (0.31 ± 0.12 eV) and $T_{trans,2} = 550 \pm 250$ K (0.095 ± 0.043 eV).

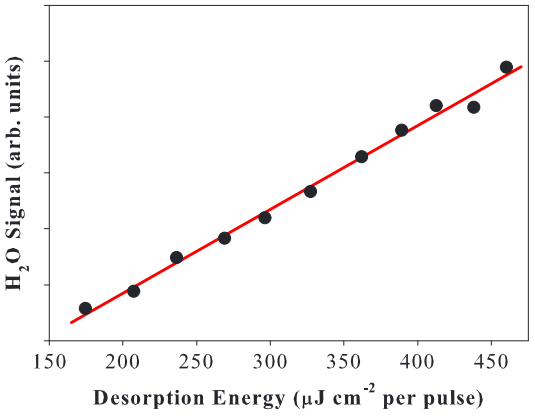

Figure 5. H_2O desorption signal from 10 L ASW on lunar slab as a function of desorption energy per pulse. Best fit line is shown. TOF = 1.7 μs.

As shown in our previous work [*DeSimone et al.*, 2013], an alternate method of fitting the data that yield a wider distribution, by integrating over the desorption laser spot, was unsubstantiated by experiments. However, it theoretically makes sense that the distribution should be wider when all desorption trajectories are included instead of assuming that all water molecules leave normal to the surface.

Figure 4 shows the data from Figure 3 after the Jacobian transformation to velocity space. The Maxwell-Boltzmann distributions were calculated using equation (2) with $T_{trans,1} = 1800$ K, $T_{trans,2} = 550$, $T_{trans,3} = 102$ K, and $r = 2$ mm. The peak of the total velocity distribution fit for 2 L ASW on the lunar slab corresponded to a velocity of ~950 m/s, which was also the most

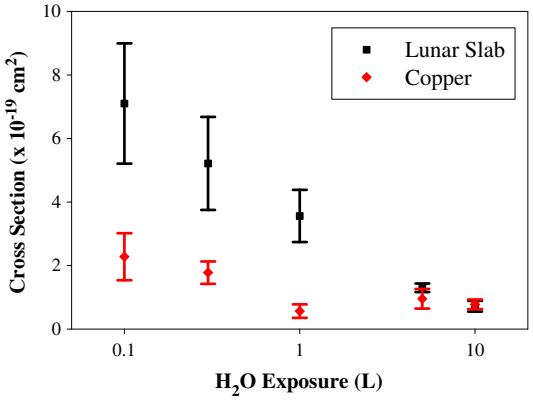

Figure 6. Water removal cross sections for various H_2O exposures at 102 K on the lunar slab. Error bars represent 90% confidence intervals. For comparison, cross sections are also shown on copper (probably coated with a thin oxide layer).

common velocity of H_2O ($v = 0$) desorbing from 600 L ASW [*DeSimone et al.*, 2013].

Desorption signal was found to be linear with respect to desorption laser flux. This result was already shown for thick ASW with desorption energies below 100 μJ cm^{-2} [*DeSimone et al.*, 2013], but signal was much smaller for low H_2O exposures on the lunar slab. Consequently, higher desorption energies were required to obtain adequate signal-to-noise ratios. Figure 5 shows that water signal at TOF = 1.7 μs increases linearly with desorption energy per pulse, so a single-photon mechanism of desorption is indicated. Water removal cross sections were measured at 0.1, 0.3, 1, 5, and 10 L H_2O exposures, and they were found to increase with decreasing coverage. Figure 6 shows cross sections for water removal on the lunar slab and on the copper sample holder, which probably has an oxidized surface, for comparison. No corrections were made to the cross sections to account for different surface areas because the cross section for 10 L H_2O on the lunar slab, $(7.2 \pm 1.7) \times 10^{-20}$ cm^2, matched that for 10 L H_2O on the sample holder. The 5 L cross section on the lunar slab, $(1.3 \pm 0.1) \times 10^{-19}$ cm^2, was slightly higher than on the sample holder. As expected, the most profound differences occurred at low coverages. For example, the 1 L cross section for H_2O removal from the lunar slab, $(3.6 \pm 0.8) \times 10^{-19}$ cm^2, was almost an order of magnitude greater than the 1 L cross section for H_2O removal from the sample holder.

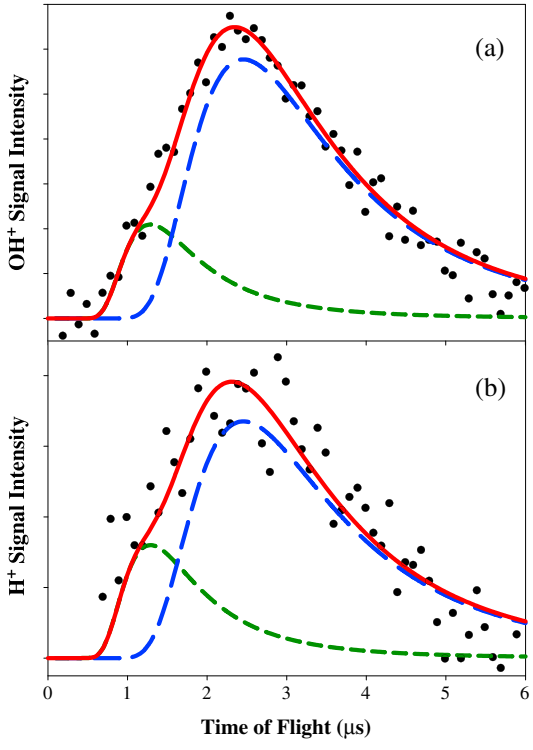

Figure 7. TOF spectra of (a) OH^+ and (b) H^+ fragment ions from vibrationally excited H_2O molecules desorbed by 157-nm photons from 5 L ASW on the lunar slab at 102 K. Maxwell-Boltzmann distributions with $r = 3.5$ mm and $T_{trans} = 1100$ K (blue dashes) and 4000 K (green dashes) sum to the total fit (red line) of the data (black circles).

While predissociation made direct detection of H_2O (v^*) impossible, TOF spectra for the H^+ and OH^+ fragments from vibrationally excited water were detected via nonresonant ionization at 253 nm. The Maxwell-Boltzmann distributions shown in Figure 7 were calculated according to equation (1) with $T_{trans,1} = 4000$ K, $T_{trans,2} = 1100$ K, and $r = 3.5$ mm. These TOF spectra were very similar to those from thick ASW on the sample holder [*DeSimone et al.*, 2013]. However, as with the TOF spectra for H_2O ($v = 0$), there was some additional fast signal that could not be explained by off-normal trajectories, collisions, pores, and surface roughness. Consequently, the data were fit with two components, which may correspond to the two primary categories of adsorption geometries: oxygen down and oxygen up.

OH^+ signal at the peak of its TOF spectrum was monitored as a function of irradiation time. For 5 L H_2O exposure, OH^+ signal increased until irradiation

by ~ 5×10^{18} photons cm^{-2}. When OH^+ signal finally began to decrease, the depletion cross section was 6.4×10^{-20} cm^2. This cross section represents H_2O (v^*) removal, assuming that the entire OH^+ signal was in fact due to H_2O (v^*).

4. Discussion

4.1. H_2O Photodesorption Mechanism

Previously, for the desorption of H_2O ($v = 0$) by 157-nm irradiation of thick ASW, we supported a mechanism involving dipole reversal, in which unfavorable electrostatic interactions between the excited surface water molecule and its neighbors result in desorption [*DeSimone et al*., 2013]. Because the TOF spectrum for photodesorption of water from the lunar slab is quite similar to that of water from thick ASW, the same mechanism is likely responsible. Additionally, a small thermal component was observed from ASW on the lunar slab. This thermal component probably arises when water desorbing from within pores equilibrates to the surface temperature before finally escaping.

Complications due to pores in the lunar slab and collisions between desorbing particles make modeling these desorption events very difficult. While it is easy to imagine how off-normal trajectories and collisions can lead to lower effective translational temperatures, they should not be able to explain the large amount of desorbing water with higher translational temperatures than from thick ASW. However, different adsorption environments are available to water on the lunar substrates. Since the lunar slab is a mixed metal oxide, there are many different adsorption sites available to water molecules, so a variety of desorption energies is expected. The strength of the interaction between a water molecule and the substrate can affect the energy with which the water molecule desorbs by changing the relevant potential energy surfaces. For example, when the excited water molecule is surrounded by metal cations and oxygen anions instead of by other water molecules, the excitation may remain more localized, and the dipole reversal mechanism may lead to even stronger repulsion between the water molecule and the surface. Because there are two primary categories of adsorption geometries, either interacting with the surface through oxygen or through hydrogen, we have chosen to lump the desorbing water into two nonthermal components. However, the reality of water adsorption on these surfaces is much more complicated, as different metal ions undoubtedly affect water adsorption differently.

Photodesorption of H_2O (v^*) may be due to several different mechanisms: dipole reversal, kickout, and recombination of hydroxyls. The formation of H_2O (v^*) is likely due to at least in part to recombinative desorption of photofragments because signal indicative of H_2O (v^*) increases with irradiation time. Our companion paper focuses on the $O(^3P)$ fragment, which also increases with irradiation time and is primarily formed by hydroxyl recombination [*DeSimone and Orlando*, 2014b]. In fact, for 5 L H_2O exposure, signals indicative of $H_2O(v^*)$ and $O(^3P)$ both increase for 5×10^{18} photons cm^{-2} and then decrease with similar cross sections, so it is plausible that both signals arise from the same mechanism. As photodissociation occurs, more OH radicals become available for recombination: $OH + OH \rightarrow H_2O + O$. The resulting water molecules are predicted to exhibit significant vibrational excitation [*Andersson et al*., 2011].

4.2. Water Removal Cross Section

The cross sections for water removal at low coverages were higher on the lunar slab than on the oxidized copper sample holder, possibly due to differing interactions between water and the two substrates. Coupling to a thin Cu-O layer may lead to very effective quenching of the first electronic state of water. When quenching occurs more quickly, there is less time for the excited water molecule to gain momentum while on the repulsive potential energy surface, so desorption is less likely. We recognize that copper with a thin oxide overlayer is not the best material to compare to the lunar slab, but it is present on the sample holder and is the substrate used in our previous work, which primarily focused on thick ASW independent of the substrate [*DeSimone et al*., 2013]. As another point of comparison, photodesorption of monolayer water ice on amorphous carbon was measured for 193 nm irradiation to have a cross section of $(7.4 \pm 0.5) \times 10^{-19}$ cm^2 [*Mitchell et al*., 2013]. This value is quite similar to our measured 0.1 L cross section on the impact melt breccia, $(7.1 \pm 1.9) \times 10^{-19}$ cm^2, despite the lower photon energy.

When charge transfer between a water molecule and the lunar surface occurs, the equilibrium geometry of the adsorbed water molecule changes. This altered geometry can lead to an excited state potential energy

surface that is accessible in the Franck-Condon region at lower photon energies relative to gas phase water. In this case, 7.9 eV photons could be near the peak of the first absorption band rather than on the edge, so more desorption could occur. The 7.9 eV photons may also create mobile excitons within the metal oxide substrate. These excitons can diffuse to the surface over a typical distance of about 50 nm and become trapped on a surface water molecule, though defects in the substrate can reduce this distance. This exciton can lead to the same singlet excited state of water as direct photoexcitation as well as a triplet state. These excited states can lead to subsequent desorption or dissociation.

Differences in quenching and delocalization rates at different H_2O exposures can also explain why cross sections increase with decreasing exposure on both substrates. Delocalization of the excited state is very rapid within defect-free ice, as the exciton diffuses easily along hydrogen bonds. For low exposures, quenching of the excited state is less rapid, and delocalization is limited. Thus, the excited state lifetime increases, and there is more time for the excited water molecule to accelerate away from the surface while on the repulsive potential energy surface.

Because water removal cross sections increase drastically with decreasing water coverage, water is not expected to remain intact as H_2O on the sunlit lunar surface. Thermal desorption quickly removes multilayer ice at temperatures above ~ 150 K, but a wide range of desorption temperatures for chemisorbed molecular water extends up to ~ 400 K [*Hibbitts et al*., 2011; *Poston et al*., 2013]. As the lunar surface temperature varies greatly depending on the angle of incident sunlight, many locations on the Moon may contain molecular water chemisorption sites with desorption temperatures above the maximum local surface temperature. If thermal desorption were the only mechanism of water removal, H_2O adsorbed in these sites would persist. Instead, photons are likely to cause H_2O to desorb or dissociate. Therefore, the sunlit lunar surface likely contains more hydroxyls than molecular water. These hydroxyl groups are stable at lunar temperatures and will not recombine thermally below 425 K [*Hibbitts et al*., 2011; *Poston et al*., 2013]. Thermal desorption efficiently removes molecular water from the surface at temperatures above 160 K in sunlit regions of the Moon. A model of thermal desorption from a surface initially saturated with H_2O showed that the concentration of water remaining on the Moon at 60° latitude would drop below 1 ppm within eight local hour angles [*Poston et al*., 2013]. If photodesorption and photodissociation of water were included in this model, water would persist for even less time.

The branching between desorption and dissociation also depends on whether water molecules are isolated or in clusters. According to *Oberg et al*. [2009], for thick ice at 100 K, intact water desorption accounts for about 64% of the observed water removal cross section and the remaining 36% is attributed to dissociation. However, more dissociation than desorption may be expected for low coverages of H_2O on a surface. For gas phase H_2O, excitation to the first excited state is purely dissociative. However, in water hexamers, delocalization of the exciton, which facilitates desorption, occurs on the same femtosecond time scale as photodissociation [*Acocella et al*., 2012]. Since desorption requires some exciton delocalization, dissociation may be much more likely than desorption for isolated H_2O molecules on the surface. As discussed in our companion paper [*DeSimone and Orlando*, 2014b], lower H_2O exposures lead to more isolated water molecules, which are more easily photodissociated.

Therefore, the water removal cross sections for low H_2O exposures on the lunar slab are likely due in large part to photodissociation. Many of the hydroxyls formed by photodissociation eventually recombine to form H_2O (v^*) and $O(^3P_J)$. These $O(^3P_J)$ products are the focus of our companion paper, in which the cross section for $O(^3P_J)$ depletion from 5 L ASW on the impact melt breccia is reported to be 4.6×10^{-20} cm^2 [*DeSimone and Orlando*, 2014b]. Vibrationally excited water molecules can be detected indirectly via nonresonant photoionization of photofragments. Using this approach, the cross section for H_2O (v^*) depletion from 5 L ASW on the impact melt breccia was found to be 6.4×10^{-20} cm^2. It is not surprising that this value is similar to the cross section for $O(^3P_J)$ depletion since both the $O(^3P_J)$ and H_2O (v^*) yields depend on the concentration of adsorbed hydroxyls.

The approximate density of water in the desorption plumes can be estimated from the measured cross sections. For example, the cross section for 1 L exposure was 3.6×10^{-19} cm^2, and the typical photon flux was 2×10^{14} photons cm^{-2} per pulse. Multiplying the cross section by the photon flux and the surface coverage (10^{15} molecules cm^{-2}) reveals that 7×10^{10} molecules cm^{-2} either desorb or dissociate during each

desorption laser pulse, so 7×10^{10} molecules cm^{-2} is an upper limit to the density of water directly above the surface. These molecules spread out according to the measured velocity distribution, so the volumetric density is constantly changing. Although this density is probably higher than that above the lunar surface due to the much higher photon flux in our experiment, our results are still relevant to the Moon because cross sections are calculated on a per-photon basis, and no multiphoton processes are indicated by Figure 5. The experimentally indicated desorption mechanisms and cross sections should be applicable to the lunar surface since desorption yield increases linearly with photon flux.

4.3. Implications for Water on the Moon

At the low coverages of water that may be present on the sunlit lunar surface (up to 1000 ppm) [*Clark*, 2009], the most applicable cross section we measured is for 0.1 L ASW. While 1000 ppm may seem like a large number, remember that thick ASW contains 1,000,000 ppm water. The water deposited in these experiments generally adsorbs on top of the surface rather than implanting within it as a solar wind proton might, so we do not need to dose much water to achieve surface concentrations similar to those that might exist on the Moon. Solar wind proton implantation generally produces OH and only potentially produces H_2O under extremely saturated conditions. If a water molecule were formed at depths of 10–100 nm, it is unlikely that photodesorption could occur through the dipole reversal mechanism described above, as quenching of the excited state would be fast compared to diffusion out of the regolith. Indeed, no subthermal signal, which would indicate diffusion, is observed in the H_2O TOF spectra. Because the present experiments involved only water deposited on top of the surface and not hydrogen atoms implanted in the lunar material, caution must be exercised when applying the measured cross sections to water-equivalent hydrogens on the Moon. The water must be adsorbed on top of the lunar surface, not implanted deep within the regolith, in order for these cross sections to be appropriate.

We can estimate the removal/destruction rate of H_2O, R_{H2O}, on the lunar surface by ultraviolet photons using our measured 0.1 L cross section, $\sigma = 7.1 \times 10^{-19}$ cm^2, which includes both photodesorption and photodissociation and some assumptions based on values from the literature. The solar photon flux, F_{ph}, at the lunar surface above 8 eV is 10^{12} photons cm^{-2} s^{-1} [*Yakshinskiy and Madey*, 1999]. Our 7.9 eV irradiation is just within the first absorption band of water, and most solar photons greater than 8 eV will also be in this first absorption band and will dissociate water at similar rates.

Initial coverage depends largely on the exact location on the lunar surface. For Goldschmidt crater, which exhibited residual neutron enhancements compared to surrounding areas, 0.1–1 wt % water-equivalent hydrogen is plausible in the top layer of lunar regolith [*Lawrence et al*., 2011]. According to *Starukhina* [2012], these hydrogen atoms are generally found in the top 100 nm of lunar regolith even though neutron spectroscopy probes millimeters in depth. The following expression may be used to estimate the concentration of water-equivalent hydrogen near the surface (n_s):

$$n_s \approx \frac{2q}{Sm_H\mu_W} = 6.6 \times 10^{16}\,cm^{-2}, \tag{3}$$

where q is the weight ratio (0.005), S is the specific area of lunar regolith (5000 cm^2 g^{-1}), m_H is the mass of a proton, and μ_W is the molar mass of water [*Starukhina*, 2001]. If 6.6×10^{16} hydrogen atoms per cm^2 are found in the top 100 nm of regolith and we assume uniform concentration throughout these 100 nm, then the top 0.66 nm (about 1 ML) of lunar regolith should contain about 4.4×10^{14} water-equivalent hydrogens per cm^2. For this calculation, we will consider these water-equivalent hydrogens to be part of 2.2×10^{14} H_2O molecules per cm^2. The removal/destruction rate of H_2O on the sunlit surface of Goldschmidt crater due to solar photons is then

$$R_{H_2O} = F_{ph}\sigma\theta \approx 1.6 \times 10^8 \text{molecules } cm^{-2}\,s^{-1} \tag{4}$$

where θ is coverage in units of molecules cm^{-2}.

In the past, authors needing quantitative information about water photodesorption on the Moon [*Crider and Vondrak*, 2003; *Gladstone et al*., 2012] used the cross section from *Westley et al*. [1995] or the yield from *Oberg et al*. [2009], even though their laboratory studies involved thick ices on quartz and gold, respectively. Now, cross sections measured on an actual lunar substrate can be used. Future research

should determine these cross sections with Lyman-alpha photons, as additional mechanisms of water removal may occur at higher photon energies.

5. Conclusion

Desorption of H_2O ($v = 0$) following 157-nm irradiation of amorphous solid water on a lunar impact melt breccia was measured with resonance-enhanced multiphoton ionization. Photofragments of vibrationally excited water were detected with nonresonant ionization. The average cross section for H_2O ($v = 0$) removal and destruction at 0.1 L H_2O exposure was measured to be $(7.1 \pm 1.9) \times 10^{-19}$ cm^2. Cross sections were also measured at 0.3, 1, 5, and 10 L exposures. These cross sections increase dramatically with decreasing water coverage, so water is not expected to persist as molecular H_2O on sunlit portions of the lunar surface. Instead, photons are likely to cause H_2O to desorb or dissociate. Both photodissociation and solar wind implantation may lead to OH accumulation (G. A. Grieves et al., Solar wind origin and the evolution of hydroxyl on the Moon, submitted to *Geophysical Research Letters*, 2014) [*Starukhina*, 2012]. These results are also applicable to other solar system surfaces that are irradiated by solar photons, such as asteroids and interstellar silicate-based grains. As an illustration of how the measured cross sections might be utilized, the combined removal/destruction rate of H_2O on the sunlit surface of Goldschmidt crater due to solar photons was calculated to be 1.6×10^8 molecules cm^{-2} s^{-1}.

Acknowledgments
This work was supported by the NASA LASER program grant number NNX11AP13G. The authors also thank Gregory Grieves for useful discussions.

References

Acocella, A., G. A. Jones, and F. Zerbetto (2012), Excitation energy transfer and Low-efficiency photolytic splitting of water Ice by vacuum UV light, *J. Phys. Chem. Lett.*, *3*, 3610–3615.

Andersson, S., C. Arasa, A. Yabushita, M. Yokoyama, T. Hama, M. Kawasaki, C. M. Western, and M. N. R. Ashfold (2011), A theoretical and experimental study on translational and internal energies of H_2O and OH from the 157 nm irradiation of amorphous solid water at 90 K, *Phys. Chem. Chem. Phys.*, *13*(35), 15,810–15,820, doi:10.1039/c1cp21138b.

Chipman, D. M. (2006), Stretching of hydrogen-bonded OH in the lowest singlet excited electronic state of water dimer, *J. Chem. Phys.*, *124*(4), 044305, doi:10.1063/1.2162542.

Clark, R. N. (2009), Detection of adsorbed water and hydroxyl on the Moon, *Science*, *326*(5952), 562–564, doi:10.1126/science.1178105.

Colaprete, A., et al. (2010), Detection of water in the LCROSS ejecta plume, *Science*, *330*(6003), 463–468, doi:10.1126/science.1186986.

Crider, D. H., and R. R. Vondrak (2003), Space weathering effects on lunar cold trap deposits, *J. Geophys. Res.*, *108*(E7), 5079, doi:10.1029/2002JE002030.

DeSimone, A. J., and T. M. Orlando (2014a), $O(^3P_J)$ formation and desorption by 157-nm photoirradiation of amorphous solid water, accepted for publication in the *J. Chem. Phys.*, *140*, 094702, doi:10.1063/1.4867194.

DeSimone, A. J., and T. M. Orlando (2014b), Photodissociation of water and $O(^3Pj)$ formation on a lunar impact melt breccia, *J. Geophys. Res. Planets*, doi:10.1002/2013JE004598, in press.

DeSimone, A. J., V. D. Crowell, C. D. Sherrill, and T. M. Orlando (2013), Mechanisms of H_2O desorption from amorphous solid water by 157-nm irradiation: An experimental and theoretical study, *J. Chem. Phys.*, *139*(16), 164702, doi:10.1063/1.4825239.

Gladstone, G. R., et al. (2012), Far-ultraviolet reflectance properties of the Moon's permanently shadowed regions, *J. Geophys. Res.*, *117*, E00H04, doi:10.1029/2011JE003913.

Greenwood, J. P., S. Itoh, N. Sakamoto, P. Warren, L. Taylor, and H. Yurimoto (2011), Hydrogen isotope ratios in lunar rocks indicate delivery of cometary water to the Moon, *Nat. Geosci.*, *4*(2), 79–82, doi:10.1038/ngeo1050.

Hahn, P. H., W. G. Schmidt, K. Seino, M. Preuss, F. Bechstedt, and J. Bernholc (2005), Optical absorption of water: Coulomb effects versus hydrogen bonding, *Phys. Rev. Lett.*, *94*(3), 037404, doi:10.1103/PhysRevLett.94.037404.

Hama, T., A. Yabushita, M. Yokoyama, M. Kawasaki, and N. Watanabe (2009), Formation mechanisms of oxygen atoms in the O(P-3(J)) state from the 157 nm photoirradiation of amorphous water ice at 90 K, *J. Chem. Phys.*, *131*(11), 114511, doi:10.1063/1.3194797.

Hama, T., M. Yokoyama, A. Yabushita, M. Kawasaki, S. Andersson, C. M. Western, M. N. R. Ashfold, R. N. Dixon, and N. Watanabe (2010), A desorption mechanism of water following vacuum-ultraviolet irradiation on amorphous solid water at 90 K, *J. Chem. Phys.*, *132*(16), 164508, doi:10.1063/1.3386577.

Hauri, E. H., T. Weinreich, A. E. Saal, M. C. Rutherford, and J. A. Van Orman (2011), High pre-eruptive water contents preserved in lunar melt inclusions, *Science*, *333*(6039), 213–215, doi:10.1126/science.1204626.

Hibbitts, C. A., G. A. Grieves, M. J. Poston, M. D. Dyar, A. B. Alexandrov, M. A. Johnson, and T. M. Orlando (2011), Thermal stability of water and hydroxyl on the surface of the Moon from temperature-programmed desorption measurements of lunar analog materials, *Icarus*, *213*(1), 64–72, doi:10.1016/j.icarus.2011.02.015.

Hui, H. J., A. H. Peslier, Y. X. Zhang, and C. R. Neal (2013), Water in lunar anorthosites and evidence for a wet early Moon, *Nat. Geosci.*, *6*(3), 177–180, doi:10.1038/ngeo1735.

Kobayashi, K. (1983), Optical spectra and electronic structure of ice, *J. Phys. Chem.*, *87*(21), 4317–4321, doi:10.1021/j100244a065.

Korotev, R. L. (2000), The great lunar hot spot and the composition and origin of the Apollo mafic ("LKFM") impact-melt breccias, *J. Geophys. Res.*, *105*(E2), 4317–4345, doi:10.1029/1999JE001063.

Lawrence, D. J., D. M. Hurley, W. C. Feldman, R. C. Elphic, S. Maurice, R. S. Miller, and T. H. Prettyman (2011), Sensitivity of orbital neutron measurements to the thickness and abundance of surficial lunar water, *J. Geophys. Res.*, *116*, E01002, doi:10.1029/2010JE003678.

McCord, T. B., L. A. Taylor, J. P. Combe, G. Kramer, C. M. Pieters, J. M. Sunshine, and R. N. Clark (2011), Sources and physical processes responsible for OH/H2O in the lunar soil as revealed by the Moon Mineralogy Mapper (M-3), *J. Geophys. Res.*, *116*, E00G05, doi:10.1029/2010JE003711.

Mitchell, E. H., U. Raut, D. Fulvio, M. J. Schaible, C. A. Dukes, and R. A. Baragiola (2013), Ultraviolet photodesorption as a driver of water migration on the lunar surface, *Planet. Space Sci.*, *89*, 42–46, doi:10.1016/j.pss.2013.02.002.

Oberg, K. I., H. Linnartz, R. Visser, and E. F. van Dishoeck (2009), Photodesorption of ices. II. H_2O and D_2O, *Astrophys. J.*, *693*(2), 1209–1218, doi:10.1088/0004-637x/693/2/1209.

Pieters, C. M., et al. (2009), Character and spatial distribution of OH/H_2O on the surface of the Moon seen by M-3 on Chandrayaan-1, *Science*, *326*(5952), 568–572, doi:10.1126/science.1178658.

Poston, M. J., G. A. Grieves, A. B. Aleksandrov, C. A. Hibbitts, M. D. Dyar, and T. M. Orlando (2013), Water interactions with micronized lunar surrogates JSC-1A and albite under ultra-high vacuum with application to lunar observations, *J. Geophys. Res. Planets*, *118*, 105–115, doi:10.1029/2012JE004283.

Saal, A. E., E. H. Hauri, M. Lo Cascio, J. A. Van Orman, M. C. Rutherford, and R. F. Cooper (2008), Volatile content of lunar volcanic glasses and the presence of water in the Moon's interior, *Nature*, *454*(7201), 192–195, doi:10.1038/nature07047.

Sato, S., D. Yamaguchi, K. Nakagawa, Y. Inoue, A. Yabushita, and M. Kawasaki (2000), Adsorption states of NO_2 over water−Ice films formed on Au(111), *Langmuir*, *16*(24), 9533–9538, doi:10.1021/la000628n.

Starukhina, L. V. (2001), Water detection on atmosphereless celestial bodies: Alternative explanations of the observations, *J. Geophys. Res.*, *106*(E7), 14,701–14,710.

Starukhina, L. V. (2012), Water on the Moon: What is derived from the observations?, in *Moon: Prospective Energy and Material Resources*, edited by V. Badescu, pp. 57–85, Springer, New York.

Sunshine, J. M., T. L. Farnham, L. M. Feaga, O. Groussin, F. Merlin, R. E. Milliken, and M. F. A'Hearn (2009), Temporal and spatial variability of lunar hydration as observed by the deep impact spacecraft, *Science*, *326*(5952), 565–568, doi:10.1126/science.1179788.

Westley, M. S., R. A. Baragiola, R. E. Johnson, and G. A. Baratta (1995), Photodesorption from low-temperature water ice in interstellar and circumsolar grains, *Nature*, *373*(6513), 405–407, doi:10.1038/373405a0.

Yakshinskiy, B. V., and T. E. Madey (1999), Photon-stimulated desorption as a substantial source of sodium in the lunar atmosphere, *Nature*, *400*(6745), 642–644.

Zimmermann, F. M., and W. Ho (1995), State-resolved studies of photochemical dynamics at surfaces, *Surf. Sci. Rep.*, *22*(4–6), 127–247, doi:10.1016/0167-5729(96)80001-X.